NASA-TM–2017–219370

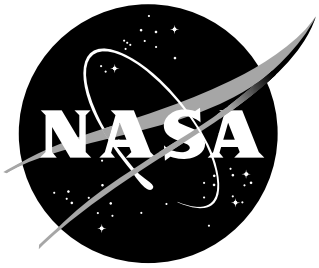

Examination of a Rotorcraft Noise Prediction Method and Comparison to Flight Test Data

D. Douglas Boyd, Jr., Eric Greenwood, Michael E. Watts, Leonard V. Lopes
Langley Research Center, Hampton, Virginia

January 2017

NASA STI Program . . . in Profile

Since its founding, NASA has been dedicated to the advancement of aeronautics and space science. The NASA scientific and technical information (STI) program plays a key part in helping NASA maintain this important role.

The NASA STI program operates under the auspices of the Agency Chief Information Officer. It collects, organizes, provides for archiving, and disseminates NASAs STI. The NASA STI program provides access to the NTRS Registered and its public interface, the NASA Technical Reports Server, thus providing one of the largest collections of aeronautical and space science STI in the world. Results are published in both non-NASA channels and by NASA in the NASA STI Report Series, which includes the following report types:

- TECHNICAL PUBLICATION. Reports of completed research or a major significant phase of research that present the results of NASA Programs and include extensive data or theoretical analysis. Includes compilations of significant scientific and technical data and information deemed to be of continuing reference value. NASA counter-part of peer-reviewed formal professional papers but has less stringent limitations on manuscript length and extent of graphic presentations.
- TECHNICAL MEMORANDUM. Scientific and technical findings that are preliminary or of specialized interest, e.g., quick release reports, working papers, and bibliographies that contain minimal annotation. Does not contain extensive analysis.
- CONTRACTOR REPORT. Scientific and technical findings by NASA-sponsored contractors and grantees.
- CONFERENCE PUBLICATION. Collected papers from scientific and technical conferences, symposia, seminars, or other meetings sponsored or co-sponsored by NASA.
- SPECIAL PUBLICATION. Scientific, technical, or historical information from NASA programs, projects, and missions, often concerned with subjects having substantial public interest.
- TECHNICAL TRANSLATION. English-language translations of foreign scientific and technical material pertinent to NASAs mission.

Specialized services also include organizing and publishing research results, distributing specialized research announcements and feeds, providing information desk and personal search support, and enabling data exchange services.

For more information about the NASA STI Program, see the following:

- Access the NASA STI program home page at http://www.sti.nasa.gov
- E-mail your question to help@sti.nasa.gov
- Phone the NASA STI Information Desk at 757-864-9658
- Write to:
  NASA STI Information Desk
  Mail Stop 148
  NASA Langley Research Center
  Hampton, VA 23681-2199

NASA-TM–2017–219370

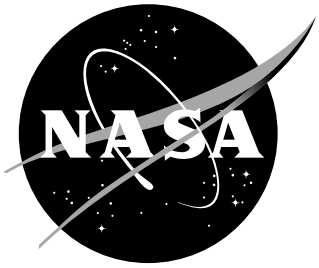

Examination of a Rotorcraft Noise Prediction Method and Comparison to Flight Test Data

D. Douglas Boyd, Jr., Eric Greenwood, Michael E. Watts, Leonard V. Lopes
Langley Research Center, Hampton, Virginia

National Aeronautics and
Space Administration

Langley Research Center
Hampton, Virginia 23681-2199

January 2017

Acknowledgments

Thanks goes to Dr. Wayne Johnson and Dr. Gloria Yamauchi of the NASA Ames Research Center for providing the initial CAMRAD II input decks and airfoil tables for the SA349/2 vehicle. This information was the starting point of the inputs used in the current work.

Available from:

NASA STI Program / Mail Stop 148
NASA Langley Research Center
Hampton, VA 23681-2199
Fax: 757-864-6500

Abstract

With a view that rotorcraft noise should be included in the preliminary design process, a relatively fast noise prediction method is examined in this paper. A comprehensive rotorcraft analysis is combined with a noise prediction method to compute several noise metrics of interest. These predictions are compared to flight test data. Results show that inclusion of only the main rotor noise will produce results that severely underpredict integrated metrics of interest. Inclusion of the tail rotor frequency content is essential for accurately predicting these integrated noise metrics.

Contents

1 Introduction

Rotorcraft are complex machines whose unique capabilities to take off vertically, land vertically, and hover make them invaluable assests to civilian and military operators. In designing a vehicle, a set of missions is chosen that essentially determines the geometric and vehicle performance quantities that are necessary to carry out the mission. Determining these quantities can be called a "vehicle sizing" task. Geometric and performance quantities for vehicle sizing comprise an optimal, consistent set of parameters (such as rotor radius, solidity, engine size and vehicle weight) that allow the vehicle to perform the desired set of missions. One such sizing methodology is the NASA Design and Analysis of Rotorcraft (NDARC) code [1] . A detailed design of many aspects of the vehicle, such as structural design of the blade, blade planform (other than gross parameters like radius and blade twist) and blade tip sweep are not included in the sizing analysis. Detailed designs are determined in a later design phase while maintaining the sizing constraints.

Once the vehicle size is determined, the size can be "frozen" and evaluated for certification, as well as various other missions that the vehicle might encounter during operations. For example, evaulating the vehicle for flight conditions required for the FAA noise certification process is important. These conditions are primarily specified in terms of power (related to engine power) instead of a specified vehicle speed. These quantities are vehicle dependent and must be determined for each vehicle design. NDARC can compute the flight condition needed to meet these power requirements.

A civilian rotorcraft design must meet a number of Federal Aviation Administration (FAA) certification standards to fly in the U.S. airspace. For example, one of these standards sets maximum vehicle noise limits for certain flight conditions. These limits are set forth in the Code of Federal Regulations (CFR) Title 14, Part 36 and are a function of gross weight: Appendix H for typical helicopters, Appendix J for "light" helicopters, and Appendix K for "tiltrotors". Appendices H and K both use the Effective Perceived Noise Level (EPNL) metric, and Appendix J uses the sound exposure level (SEL) metric to establish noise limits as a function of vehicle weight. During the design process, the goal is to compute/estimate the noise levels for FAA noise certification procedures that will be generated by a design and to examine how design changes to a vehicle will affect the noise for these procedures.

The NASA Revolutionary Vertical Lift Technology (RVLT) Project of the Advanced Air Vehicle Program (AAVP) under the Aeronautics Research Mission Directorate (ARMD), established a Technical Challenge to develop and demonstrate a multidisciplinary rotor design methodology that can design a rotor system with reduced noise while meeting other standards. For example, if a rotor blade is designed to be "low noise" (relative to the FAA noise certification limits), but is structurally

fragile and unable to meet the 2.2 lbf bird strike requirement set forth in Code of Federal Regulations (CFR) Title 14, Part 29.631, then the design is not practical.

Ultimately, a design method such as NDARC must be coupled with a noise prediction method. This coupling would allow an assessment of noise characteristics of a vehicle during the preliminary design process. The noise prediction method must be reasonably accurate and relatively fast due to the large number of iterations that are required at this design stage.

This paper examines commonly used, relatively fast, prediction tools for noise prediction of rotorcraft vehicles. This analysis method will be used to determine some key parameters that can be assessed with surrogate methods.

The method presented in this work can be used in a "standalone" analysis mode, independent of any design process, or be used in an optimization process, such as OpenMDAO [2], to examine the effects of changes in parameters or configuration on noise metrics.

After developing the noise prediction methodology, the next step is to validate the predictions. The primary purpose of this work is to examine this prediction capability. Because rotorcraft are required to meet EPNL noise limits set forth in the FAA noise certification process, the current work will examine predictions of EPNL, as well as a number of other common noise metrics, for a configuration of interest. This examination will use codes and methods that are typical of ones in use by many organizations today. Predictions will be compared to data from a recent flight test of a conventional rotorcraft (main rotor and tail rotor) that has already been through the FAA noise certification process.

A similar study was performed by Snider et al. [3]; however, that work primarily was intended to show that a broadband noise model is necessary in order to accurately compute the measured EPNL values measured during FAA noise certification. Reference [3] used specific codes that are Bell Helicopter Textron in-house proprietary codes. Though good results were shown, a similar benchmarking method is performed here for analyses currently used by NASA, all of which are different from the codes used in Reference [3]. Similiar to Reference [3], the current work will examine the ability to compute EPNL for a vehicle of interest, but will not focus on reproducing specific FAA noise certification flight conditions. Requirements to accurately compute EPNL, as well as a number of other metrics of interest, from a flight test will be investigated.

In the following sections, the vehicle used in this work and the prediction method for the vehicle trim, airloads, and noise prediction will then be described. Finally, comparisons will be made between the prediction and the data.

2 Prediction Method

2.1 Trim, blade motion, blade loads

For a conventional rotorcraft configuration with main and tail rotors, the two rotors are typically the primary noise sources. Prediction of rotorcraft acoustics from these rotors requires knowledge of the blade motion and the loads on the blades. To know the blade motion and loading, knowledge of the rotorcraft trim state is required. The trim state of a rotorcraft typically includes rotor controls and the vehicle orientation, which are consistent with the given flight path.

The current state-of-the-art for predicting the rotorcraft trim state for a given flight condition is often embodied in a "comprehensive analysis," which accounts for rotor and rotorcraft aerodynamics and dynamics. In the current work, the second generation Comprehensive Analytical Model of Rotorcraft Aerodynamics and Dynamics (CAMRAD II) [4] is used to compute the rotorcraft trim state for a given flight condition. The items shown in Figure 1 such as the vehicle geometry (which includes items such as the configuration, and number and orientation of the rotors) and the vehicle flight condition, are used as input to CAMRAD II.

CAMRAD II includes a finite element beam model, lifting line aerodynamics model for the rotor blades, airframe aerodynamics models, a number of wake models (i.e., uniform inflow, prescribed or rigid wake, free wake), and solution procedures that solve these models to achieve the trim state of the vehicle consistent with the desired flight condition. CAMRAD II also has the ability to perform flutter-related calculations, which include items such as eigenvalues, eigenvectors, and blade model shapes. In addition, a transient analysis task is available to compute the response of the rotorcraft system to inputs, such as a change in collective stick position, and gust. For the computations in the present work, only the CAMRAD II trim analysis is employed.

Given geometric, fuselage aerodynamic, blade sectional aerodynamic, and structural information of a rotorcraft configuration, CAMRAD II determines the trim state of the vehicle for a specified flight condition. For the cases in this paper, the trim state is defined as a set of controls - main rotor collective and cyclic pitch settings and vehicle orientation - necessary to achieve the desired flight condition. The steady flight condition for these cases is defined by providing the vehicle velocity, climb angle, and vehicle weight. The rotor blades are assumed to be rigid. This assumption is due to the lack of available information about elastic properties of the blades on the specific flight vehicle used in this work. This is not a limitation of the current method - the exact same method is applied whether the rotor blades are elastic or rigid.

Once the trim state is determined, blade motion, vehicle orientation, and blade loading are available for further analysis. A "converter" pro-

gram is used to read the CAMRAD II output, extract the data (blade motion and blade loading), and reformat the data into a specific set of data files that are used by the noise prediction method. The noise prediction method uses features available in the second generation Aircraft NOise Prediction Program (ANOPP2) [5]. An outline of the prediction method is presented graphically in Figure 1.

2.2 Noise Prediction

Given the vehicle trim state, the blade motions and lifting line blade forces as a function of radius and azimuth (for each rotor) are extracted from CAMRAD II results. The general noise prediction scheme includes computation of the acoustic pressure time history at a set of observer locations. From the acoustic pressure data, quantities such as power spectral density (PSD) spectrum, narrowband spectrum (NB), one-third octave band sound pressure level spectrum (1/3-octave), and overall sound pressure level (OASPL) can be computed. For a flyover simulation, the acoustic pressure time history at a set of observers located on a hemispherical surface below the vehicle is computed first. Each of these time histories is converted into a 1/3-octave band sound pressure level spectrum. This hemisphere of spectral data is then "flown" along a flight path trajectory and a time history of frequency integrated metrics, such as the perceived noise level (PNL) and tone-corrected perceived noise level (PNLT), are computed at another observer location, such as a stationary observer on the ground. These spectral time histories at the ground observer locations can be further integrated to obtain time integrated metrics, such as EPNL, unweighted sound exposure level (SEL-u), and A-weighted SEL (SEL-A).

The above noise prediction tasks are performed by way of an "ANOPP2 user code" as indicated in Figure 1. This user code was written to accept information such as the flight path, observer locations, atmosphere, acoustic data surface information (impermeable, permeable, and compact line methods are available) and instruct ANOPP2 to compute the desired acoustic quantities.

2.2.1 Discrete Frequency Noise on a Hemisphere Under the Vehicle

Computation of the acoustic pressure time history at each observer location is performed by solving the Ffowcs Williams-Hawkings equation using Farassat's Formulation 1A ("F1A") [6] capability within ANOPP2, coined ANOPP2-F1A. ANOPP2-F1A computes the acoustic pressure time history using blade geometry, blade motion, and lifting line forces on the rotor blades [5, 7]. The lifting line method in CAMRAD II does not use the airfoil section shape; instead, the airfoil sectional aerodynamics are interpolated from a table containing lift, drag, and pitching

moment coefficients as as function of angle of attack and Mach number. To approximate the thickness noise, a symmetric NACA airfoil section with the same maximum thickness of the actual airfoil section is used. It is also required that the cross-sectional area be the same to match thickness noise; however, because the maximum thickness and the chord length are matched with the actual section, it is assumed here that the cross-sectional area difference between the modeled airfoil and the actual airfoil is small. Because the loading data available are sectional forces on the rotors as a function of rotor radius and azimuth location, the compact chordwise version of ANOPP2-F1A is used for computation of the acoustic pressure time history components that are attributable to the blade loading. The compact chordwise loading is applied on the quarter-chord of the blade section.

2.2.2 Additional Broadband Hemisphere

For a vehicle flyover, the acoustic pressure time history for a set of observers on a hemispherical surface under the rotorcraft is computed first. A 1/3-octave band sound pressure level spectrum is then computed at each observer location on the hemisphere and is available for use in the subsequent flyover simulation.

An optional hemisphere can then be included in the analysis. This optional hemisphere consists of a modified broadband noise model based on the Pegg model [8]. This model, as currently implemented in the ANOPP2 user code, is only available for the main rotor (which is assumed to be the first rotor). Other broadband noise sources, such as engine noise, are not included. A simple scale factor is applied to the noise spectrum generated by the standard Pegg model. As the Pegg model is an empirically-based model, the scaling parameter included in the current model is simply another empirical constant that can be adjusted to best match measured data. For a scaling factor value of 1, the original Pegg model is recovered.

This additional 1/3-octave hemisphere is added to the 1/3-octave hemisphere that was obtained in the earlier part of the computation using CAMRAD II and the ANOPP2-F1A. This process creates a single 1/3-octave hemisphere which contains the thickness and loading noise from all rotors and the main rotor broadband noise.

2.2.3 Noise from a Flyover

The new single hemisphere is then "flown" along a flight path. For the current work, the flight path is assumed to be a straight line through a constant-property atmosphere at specified atmospheric conditions. The straight-line flight path can be a level flyover at a constant height above the ground. The path can also be at a climb angle or descent angle that intersects a point at a user-given height above the ground origin point

(0,0,0).

As this hemisphere is flown along a trajectory, noise is computed at an observer location using the straight ray method of ANOPP implemented in ANOPP2 (called "ANOPP2-AnoppGround"). In the cases examined here, the observer is stationary and on the ground. The noise at this location, provided by ANOPP2-AnoppGround, is effectively the noise from the hemisphere that would reach the ground observer, taking into account effects such as hemisphere motion ("Doppler effect"), atmospheric absorption and attenuation, and spherical spreading. The ground observer data for a flyover is then composed of a time history of spectral data at 0.5-second intervals during the flyover. These spectral data are then provided to ANOPP2's Acoustic Analysis functionality to calculate frequency-integrated metrics such as PNL, PNLT, and OASPL, as well as time-integrated metrics such as EPNL, SEL-u, and SEL-A.

3 Measured Data

Between September 2014 and February 2015, a series of flight tests was conducted by NASA and the U.S. Army Aviation Development Directorate (ADD) [9]. The primary objectives of the test series were to (1) determine the effects of varying ambient conditions and gross weight on noise generation (2) gather data to aid in development, implementation, and improvement of prediction codes and methodologies. The vehicle used was a Eurocopter AS350 SD1 rotorcraft. Some of the vehicle characteristics of this single engine, light helicopter are summarized in Table 1.

Table 1. AS350 SD1 Characteristics.

Main Rotor		
Number of blades	3	
Radius	5.345	meters
Chord	0.350	meters
Nominal RPM	394	
Linear Twist Rate	-8.4	degrees
Max blade thickness	0.09	% chord
Airfoil section	OA209	
Tail Rotor		
Number of blades	2	
Radius	0.930	meters
Chord	0.1855	meters
Nominal RPM	2086	
Linear Twist Rate	0.0	degrees
Max blade thickness	0.12	% chord
Airfoil section	NACA 0012	
Vehicle		
Gross Weight	1996	kilograms

Various flight conditions were flown during the flight test series. Two conditions will be used here to examine the ability of current prediction methods to compute various acoustic quantities, such as EPNL. The two test conditions used here - a level flight case and a descent flight case - are described in Table 2 together with the atmospheric conditions that were used in the predictions. The average speed and average climb angle were deduced from the measured tracking data.

In addition to the EPNL shown in Table 2, Table 3 provides a list of other integrated noise metrics such as the SEL-u, SEL-A, unweighted Equivalent Continuous Sound Level (Leq), A-weighted Equiv-

alent Continuous Sound Level (Leq-A), unweighted Maximum Sound Level (Lmax), and A-weighted Maximum Sound Level (Lmax-A), which were computed from measured acoustic pressure time histories. As used in this study, the terms "unweighted SEL" and "A-weighted SEL" are technically the "unweighted Single Event Noise Exposure Level (unweighted SENEL)" and "A-weighted Single Event Noise Exposure Level (A-weighted SENEL)", respectively. The difference is that, by definition, the SEL quantities are integrated between two instances in time. The SENEL values, however, are integrated between the time instances defined by the times when the noise metric is 10 dB lower than the maximum noise metric value. The FAA certification process shows the definition of the SEL quantity, but then indicates that the two time instances are "in practice" set by the times for which the noise metric is 10 dB below the maximum value of the noise metric. The maximum noise metric is defined as Lmax (for unweighted quantities) or Lmax-A (for A-weighted quantities). Leq is defined as the constant noise level for the entire flyover which is equivalent to the unweighted SEL value for that flyover. Likewise, Leq-A is defined as the constant A-weighted noise level for the entire flyover which is equivalent to the A-weighted SEL value for that flyover. For this document, the commonly used definition of the SEL quantity (which, is actually the SENEL value) is used. The terminology SEL is also retained, per common practice.

Table 2. Flight Conditions.

Level Flight		
Run Number	302248	
Average True Air Speed	92.5	knots
Average Climb Angle	-0.39	degree
Height AGL at overhead	109.62	meters
EPNL	93.13	EPNdB

Descent Flight		
Run Number	273104	
Average True Air Speed	98.4	knots
Average Climb Angle	-5.17	degree
Height AGL at overhead	74.378	meters
EPNL	93.67	EPNdB

Atmosphere		
Density	1.05489	kilogram/meter^3
Temperature	12.83	Celsius
Pressure	85,900.	Pascals
Speed of Sound	339.01	meter/second

Table 3. Measured Noise Metrics.

Level Flight		
EPNL	93.13	EPNdB
SEL	99.31	dB
SEL-A	89.01	dBA
Leq	89.10	dB
Leq-A	81.23	dBA
Lmax	92.54	dB
Lmax-A	84.34	dBA

Descent Flight		
EPNL	93.67	EPNdB
SEL	99.93	dB
SEL-A	91.10	dBA
Leq	90.15	dB
Leq-A	82.07	dBA
Lmax	94.62	dB
Lmax-A	85.47	dBA

4 Modeling of the Vehicle in CAMRAD II

As a starting point, the CAMRAD II model for the AS350 SD1 began as CAMRAD II input decks for the SA349/2 vehicle as provided by Dr. Wayne Johnson and Dr. Gloria Yamauchi of the NASA Ames Research Center and was based on References [10] and [11]. However, there are a number of major differences between the SA349/2 and the AS350 SD1 used in the current work. The original input decks were modified to create a new input deck for the AS350 SD1 helicopter using data from Reference [12]. The major changes are outlined below.

For the main rotor, the rotor radius, chord, solidity, tip speed, and RPM were updated. For the blade structural model, the blades were considered rigid, so no elastic properties were required. The methods used behave the same whether the blades are elastic or rigid - only the internal calculations of CAMRAD II are affected. The reason for using the rigid blade assumption was that the elastic blade properties were not readily available for the current blades. The blade mass was adjusted to match the measured blade mass. The blades have a linear twist of 8.4 degrees from the center of rotation to the tip. Aerodynamic sectional information for the main rotor was extracted from airfoil tables of lift, drag, and pitching moment for the OA209 airfoil.

For the tail rotor, the original SA349/2 model included a fenestron. However, the AS350 SD1 vehicle is equipped with a two-bladed tail rotor that consists of an untwisted, rectangular planform with NACA 0012 symmetric airfoils. In addition, the gear ratio of the tail rotor was set such that the RPM of the tail rotor was matched to the measured tail rotor RPM of the level flight case, determined from analysis of the acoustic data. Tail rotor radius, chord, solidity, and blade mass were matched to measured values. Aerodynamic sectional information was determined from an airfoil table of lift, drag, and pitching moment for the NACA 0012 airfoil.

The airframe aerodynamics model was assumed to be the same as the original SA349/2. The airframe elasticity model was not used.

The main rotor collective pitch, lateral pitch, longitudinal pitch, fuselage pitch, fuselage roll, and pedal control (effectively, the tail rotor collective) were used to trim the three forces and moments acting on the free flight vehicle at the given flight condition.

5 Level Flight

5.1 Acoustic Pressure Time Histories

The acoustic pressure time history is the fundamental quantity measured at a microphone location during an acoustic flight test. Acoustic metrics of interest are derived from this quantity. The acoustic pressure time history is examined when assessing a prediction method that is based on the time domain rather than on the frequency domain. This section assesses the prediction of the acoustic pressure time history compared to measurements.

The acoustic pressure time history is predicted and compared to measured data from six locations of the vehicle along the flight track. The tracking data from the flight test is used to locate the relative position of the vehicle and microphone. The measured microphone data is from a stationary microphone (with the vehicle moving). For all predictions in this work, data from "Microphone 10" is used because it is close to the centerline of the flight track for both the level flight case examined in this section and for the descent case examined subsequently.

Figure 2 shows the measured and predicted acoustic pressure time histories for six locations, corresponding to 5, 3, and 1 second prior to the vehicle being directly over the microphone 10 location and 1, 3, and 5 seconds after the vehicle has passed microphone 10.

For convenient angular reference, the title above each figure indicates the "polar angle", θ, between (1) a line pointing forward from the vehicle and is parallel to the ground plane and (2) the microphone location. With this polar angle definition, for polar angles between $\theta = 0°$ and $90°$, the microphone is in front of the vehicle, and for polar angles between $\theta = 90°$ and $180°$, the microphone is behind the vehicle.

At $\theta = 19°$, it is seen that the measured data is dominated by pulses indicative of thickness noise. The smaller, more frequent peaks are from the tail rotor, and the larger peaks are from the main rotor. In the analysis, the main rotor RPM was set to 396.5 based on the spacing of the known main rotor thickness pulses in the measured data. This value is within 1% of the nominal RPM of 394 and is well within the RPM variation measured during the flight test. The tail rotor RPM was set to 2088.56, based on spacing of the known tail rotor pulses in the measured data. In Figure 2, the black lines are the measurements and the red lines are the predictions. The x-axis shows a time spanning one main rotor revolution. Because the exact location of the rotor blades is not known in the measurement (unknown azimuth location relative to the measured time on the x-axis), the predictions were shifted in time by small amounts to align the thickness noise peaks.

The predictions match the measured data well in phase and amplitude. However, the analysis overpredicts the blade vortex interactions (BVI) just prior to the main rotor pulse. There are several reasons for

this overprediction. First, the comprehensive analysis requires input of a vortex core radius for the tip vortex. In this case, the tip vortex core size is held constant and is equal to 1.0 chord. While this is a large value compared to actual vortex core sizes, a large size is required in the computation to avoid even larger overshoots in the BVI magnitude. Also, the orientation of the main rotor is an important factor in the location and strength of the BVI events. For this case, the main rotor tip path plane orientation is not known precisely, so the predicted, trimmed main rotor tip path plane orientation is assumed to be correct.

At $\theta = 30°$, the predictions still match the location of the main and tail rotor thickness pulses, but the measured pulses are becoming sharper and more nondeterministic noise sources are starting to show. As with $\theta = 19°$, the predicted BVI event just prior to the main rotor thickness pulse is stronger than in the measured data. At $\theta = 63°$, the predictions and measurements show the same trends as $\theta = 30°$; however, the measured data has more content that appears to be high frequency and nondeterministic.

After the vehicle passes the microphone location ($\theta = 117°, 150°$, and $162°$), a 3 per revolution ("3p") feature appears with a large amount of nondeterministic, broadband noise on top of the 3p feature. The prediction shows this 3p content well, but is void of the high frequency, broadband noise evident in the measurements because the time domain prediction method does not include broadband noise. For $\theta = 150°$ and $162°$, the measured data are also dominated by broadband noise with evidence of a thickness-like pulse from the main rotor. The predictions mimic the measured data well, except for the broadband noise content.

5.2 One-third Octave Band Sound Pressure Level Spectra

Figure 3 shows the unweighted one-third band sound pressure level spectra (predicted for the main rotor harmonic noise only compared with measured data for the complete vehicle) at the same time locations examined in Figure 2. As with Figure 2, only the discrete frequency noise is predicted.

The spectral shape of the low- and mid-frequency noise is reasonably well predicted for $\theta = 19°, 30°$, and $63°$, with overprediction at the highest frequencies. The spectral shape of the low- and mid-frequency noise is reasonably well represented, but the levels are underpredicted. The highest frequencies are typically not of interest because they are quickly attenuated by the atmosphere.

For $\theta = 117°, 150°$, and $162°$, the low frequency content is well predicted, but the mid-frequency content is substantially underpredicted. This result is expected because the predictions do not account for broadband noise.

Figure 4 shows the same measured data as Figure 3, but the predictions now include broadband nosie computed with a modified Pegg

model. The modifed Pegg model (described in section 2.2.2) with scale factor set to 0.91 was used. The origin of this 0.91 factor is explained below in Section 5.4. As expected, relative to Figure 3, the mid-frequency noise content is increased in the locations after the vehicle has passed the microphone.

Figure 5 shows results of Figure 4 with the tail rotor noise included. The two primary effects of the tail rotor are to increase the low-frequency noise content and to decrease the high-frequency content prior to the vehicle passing over the microphone. The effects are more pronounced when the vehicle is nearly above the microphone location ($\theta = 30^\circ$ and 63°).

5.3 Unweighted Overall Sound Pressure Levels During Flyover

Figures 3 through 5 showed individual spectra at 6 discrete points under the flight spanning a time period between 5 seconds before and after the vehicle is directly above microphone 10. To see a broader picture of how the measured and predicted data compare, the acoustic pressure time history is sampled every 0.5 seconds. At each of these sampling times, the sound pressure level spectrum is computed. The sound pressure level spectrum is then integrated at each of these times to obtain an overall sound pressure level (OASPL) [dB] level. Figure 6 shows the unweighted OASPL as the vehicle flies over the microphone. This figure only includes the main rotor. The x-axis is the "Reception Time", t (in seconds), and can be considered the time relative to the vehicle being directly over microphone 10. For t $<$ 0 seconds, the vehicle is approaching the microphone. For t $>$ 0, seconds the vehicle has passed the microphone and is departing. So, for t $<$ 0 seconds, the microphone data represent noise events projected in front of the vehicle. For t $>$ 0 seconds, the microphone data represent noise events aft of the vehicle. The peak value Figure 6 shows that on approach, main rotor thickness noise is the largest component of the prediction, and the loading noise is a small part of the noise until approximately t = -4 seconds. At that time, the thickness noise drops significantly and the loading noise becomes dominant. The broadband component at t = -10 seconds is much smaller than either the thickness or loading noise. As the vehicle approaches the microphone, the loading noise becomes the dominant noise source while the thickness noise decreases. Near t = 0 seconds, the main rotor thickness noise drops significantly and remains far below all other noise sources after the vehicle has passed overhead. This decrease in main rotor thickness noise is expected because the thickness noise is known to be small directly under the rotor. After t = 0 seconds, the forward tilt of the rotor ensures that the main rotor thickness noise remains small (as the microphone is never again near the plane of the rotor), and the primary component of the unweighted OASPL is the loading noise. Throughout the flight

track, the broadband noise is at least 10 dB below the loading noise and not a major contributor to this particular metric.

Figure 7 is similar to Figure 6, except that the tail rotor is included in the prediction. Comparing these two figures reveals that before, during, and after the vehicle has passed the microphone, the tail rotor significantly contributes to the thickness noise component. This is because the tail rotor plane is always oriented toward the microphone. The tail rotor contribution is higher on approach than on departure because of Doppler shifting of the sound. The total loading noise is mainly due to the main rotor, as the loading noise is very similar in Figures 6 and 7. Because the microphone is essentially in the plane of the tail rotor disk, the loading noise from the tail rotor is expected to be small. Including the tail rotor noise greatly improves the predicted OASPL on approach compared to the main rotor alone case, though the prediction is still approximately 2 dB below the measured value until just a few seconds before the microphone position is reached.

The broadband curve is exactly the same as in Figures 6 and 7 because only broadband noise from the main rotor is included. As mentioned previously, the broadband noise from the tail rotor is expected to be small.

Based on the comparison between Figures 6 and 7, it can be seen that including the tail rotor in the noise prediction is necessary to better capture the unweighted OASPL metric time history, especially during the approach phase of the flight.

5.4 A-weighted Overall Sound Pressure Levels During Flyover

This section shows the same flight condition as in the previous section, but instead of unweighted OASPL, the A-weighted OASPL [dBA] is examined. Because rotorcraft noise tends to be dominated by relatively low frequency noise (see the individual spectra in prior sections), examination of the unweighted OASPL indicates the ability of a prediction method to match the dominant noise sources. The A-weighting scale weights the components of noise for which the human ear is most sensitive. Examination of the A-weighted versions of Figures 6 and 7, therefore, provides an assessment of this prediction method to replicate the components of noise that are most relevant to human hearing.

Figure 8 uses the same measured data and prediction as Figure 6, but the metric is derived using A-weighted spectra. The measured data change in several ways. First, the mean level of the curve is lower for the A-weighted measured data compared to Figure 6. Second, for $t < 0$ seconds, the OASPL time history is significantly reduced compared to the unweighted values of Figure 6. These observerations suggest that there is less mid- to high-frequency content ahead of the vehicle ($t < 0$ seconds) and more mid- to high-frequency content behind the vehicle

(t > 0 seconds). The reduction of the noise metric history ahead of the rotor (t < 0 seconds) is due to the A-weighting scheme deemphasizing the lower frequency content. Behind the vehicle (when t > 0 seconds), the low-frequency noise content is small (compared to ahead of the vehicle), so the A-weighting scheme does not reduce the OASPL as much as it does ahead of the vehicle.

In general, the measured A-weighted levels are lower than the unweighted measured levels. The OASPL values on approach and departure are attenuated more at the peak value near t = 0 seconds. The predicted data generally show this same trend. However, because the very low and the very high frequencies are attenuated by the A-weighting scheme (and the mid-frequencies are emphasized), the broadband noise component - which is primarly in the mid-frequency range - is on par with and even greater than the loading noise component. The addition of these two components leads to an overprediction of the peak OASPL dBA.

Figure 9 shows the same data as Figure 8, but the A-weighted tail rotor noise is included in the prediction. Similar to the unweighted OASPL metric time history of Figure 6, the tail rotor thickness noise appears in the predictions after the vehicle has passed the microphone. Inclusion of the tail rotor has changed the frequency content of the noise emphasized by the A-weighting scheme. Some of these features are seen in the acoustic pressure time histories, which show changes in the acoustic pulses (for every main rotor thickness pulse) due to the non-integer rotational frequency of the tail rotor relative to the main rotor. The two-rotor system here will only be periodic at multiples of approximately 5.267 seconds (which is the ratio of the tail rotor to main rotor RPM) even for a steady flight condition.

Another useful metric, the sound exposure level (SEL), is an integration of the A-weighted OASPL metric time history between the time interval when the OASPL is 10 dB below the peak level (before and after the peak). Therefore, the predicted peak OASPL should be representative of the peak OASPL from the measured data. Here, because the broadband noise model is a dominant noise source for the time interval for which the SEL will be computed, a modification is made to the Pegg broadband noise level. The results of the Pegg model are multipled by a user-provided fraction that scales the Pegg model results to match the OASPL peak value.

Using Figure 9 as a guide, the Pegg model result was scaled by 0.91 (that is, reduced by 9%) to better match the SEL value resulting from integration of the measured data. Figure 10 shows the result including 0.91 Pegg model scaling. The measured A-weighted SEL value is 89.01 dBA; using the 0.91 Pegg model fraction, the predicted A-weighted SEL value is 89.09 dBA. This 0.91 fractional value is taken here as a "calibration" and will remain fixed for the remainder of this paper.

5.5 Tone Corrected Perceived Noise Levels

The tone corrected perceived noise level (PNLT) can be computed using standard procedures outlined in the Federal Aviation Regulations. These standard methods are implemented in ANOPP2 and are used in the ANOPP2 user code. The PNLT is a predecessor to the computation of the effective perceived noise level (EPNL) metric used in rotorcraft noise certification for vehicles over 7000 lb gross weight. A-weighted SEL is used for certification of vehicles below 7000 lb gross weight. Figure 11 shows the metric time history of PNLT, including the main rotor, tail rotor, and broadband noise for the main rotor (using 91% of the Pegg model value).

Consistent with results shown in previous figures, thickness noise plays a major role in the metric time history as the vehicle approaches (t < 0 seconds). The loading noise starts at a low level on approach and increases more rapidly than the thickness noise, eventually becoming more dominant than the thickness noise (from both main and tail rotors) when the vehicle is directly over the microphone. Thickness noise decreases rapidly after the vehicle has passed because the main rotor thickness noise is effectively absent and the Doppler shift reduces the tail rotor thickness noise level. The loading noise continues to play a significant role in the PNLT metric as the vehicle retreats from the microphone. The broadband noise is less significant for the PNLT metric compared to the A-weighted OASPL metric. So, broadband noise will play a major role when examining SEL metrics, but not when examining EPNL metrics.

5.6 Effective Perceived Noise Levels and Metric Summary

From the PNLT computations, an EPNL can be computed and compared to the measured value. Other metrics can also be examined for the level flight case that includes the main rotor, tail rotor, and 91% of the broadband noise model. The value of Lmax is the maximum (peak) value of the OASPL metric time history about which the SEL is integrated. The value of Leq is the constant noise level [dB] for the entire flyover, which produces the same, equivalent noise level as the SEL. There are unweighted and A-weighted versions of SEL, Lmax, and Leq, which are shown in table below. For all of the metrics shown, the unweighted values tend to be slightly lower than the measured data; whereas, the A-weighted values are slightly above the measured data. For all metrics shown, the prediction error is within approximately $\pm 2\%$ of the measured value.

Table 4. Summary of metrics for level flight case.

	Measured	Predicted	% error
EPNL	93.13	91.11	-2.2
unweighted			
SEL	99.31	97.11	-2.2
Leq	89.10	88.26	-0.9
Lmax	92.54	92.49	$\approx 0.$
A-weighted			
SEL	89.01	89.09	$\approx 0.$
Leq	81.23	82.36	1.4
Lmax	84.34	85.35	1.2

6 Descent Flight

The previous sections showed that measured data can be reproduced using a comprehensive analysis and a relatively fast noise prediction method. Using the "calibrated" model developed in the previous section for level flight, the current section will examine a descent flight condition to see if the same model can produce comparably good results relative to measured data. The flight condition in this section is the descent flight condition specified in Table 2.

6.1 Acoustic Pressure Time Histories

The same analysis procedure used for the level flight case is used to examine the acoustic pressure time histories at six vehicle locations along the flight path, relative to a centerline microphone used in the measured data. These six locations, as before, are located at 5, 3, and 1 seconds before the rotorcraft reaches the microphone location and 1, 3, and 5 seconds after the vehicle has passed the microphone location. However, note that because this is a descent flight condition, these time locations correspond to different polar angles. The polar angles again are included in the title for each figure for reference.

Figure 12 shows the calculated and measured acoustic pressure time history similar to Figure 2. At the $\theta = 30^\circ$ location, the blade passages indicative of thickness noise from the main and tail rotors are relatively well predicted. However, even at this $\theta = 30^\circ$ position ahead of the rotor, blade vortex interactions (BVI) are evident in the measured data just prior to the main rotor thickness pulse. The predictions also show that there are BVI at the same time relative to the main rotor thickness pulse, but that the amplitude of the predicted BVI is smaller than that measured. The very large vortex core radius (1.0 chords) used in CAMRAD II and set for the level flight condition could be decreased to improve this prediction. However, changing the core size for every different flight condition is not desirable when the goal is to develop a method that requires minimal user intervention during a design process. Decreasing the tip vortex core radius may improve the predictions for the descent flight case, but the predictions for the level flight case will be worse. Therefore, the core radius for the level flight case was used, and prediction of the noise metrics was assessed. For design cases where a new rotor is being developed or cases where there is not experimental data with which to calibrate a core size, the acoustic results here, and experience, indicate that a large core radius (size) is necessary for acoustic prediction. As such, in cases where the core radius cannot be calibrated with data, it is reasonable to use a core radius to be on the order of 1.0 chord in the comprehensive analysis.

Predictions at polar angles $\theta = 43^\circ$ and 74° show similar features to the results at polar angle $\theta = 30^\circ$ in that the basic thickness pulses are

predicted, and the very large, sharp BVI events are captured when the peak-to-peak value is examined. Even at $\theta = 43°$ and 74°, some broadband noise content is evident in the measurements, but is not included in the discrete frequency predictions.

The measurement at a polar angle of $\theta = 108°$ includes a large amount of broadband noise, as well as a sharp BVI event per main rotor blade passage. There is also a superimposed low frequency 3p blade loading feature. The prediction primarily shows the 3p loading feature with smaller than measured BVI events. For $\theta = 108°$ and 144° polar angles, BVI is included in the prediction, but the events are underpredicted at $\theta = 74°$ and overpredicted at $\theta = 144°$.

Broadband noise content is superimposed on a small low frequency content for $\theta = 144°$ and 160°. The predictions match the decrease in magnitude of these loading noise features, but again, do not reproduce the broadband noise content.

6.2 One-third Octave Band Sound Pressure Level Spectra

Figure 13 shows the 1/3-octave band sound pressure level spectra in a manner similar to Figure 5. For this descent case, these spectra indicate that the low frequency noise is predicted well on approach ($t < 0$ seconds) and overpredicted for the times after the rotor has passed the microphone location. Mid-frequency noise appears to be underpredicted for most times, especially after the rotor has passed over the microphone.

6.3 Overall Sound Pressure Levels During Flyover

Figure 14 shows the OASPL for the noise components for the descent flight condition. As with the level flight case, thickness noise dominates on approach and loading noise increases as the vehicle gets closer to the microphone location. Directly over the microphone, loading noise dominates, while thickness noise is less important. After the vehicle passes over the microphone, predicted loading noise dominates. Predicted broadband noise, however, is far less than either the thickness or loading noise component for this unweighted metric.

Comparing the metric time history in Figure 14 to the spectra in Figure 13, at $\theta = 30°$ and 43°, the underprediction of OASPL is due to the underprediction of the mid-frequency. The low frequency content is similar to that measured. At the polar angles of $\theta = 43°$ and 108°, the predicted low-frequency content is overpredicted, while the mid-frequency content is underpredicted. This results in the overall levels being comparable to the measured data, though the predicted components do not have quite the same distribution over the frequency range.

Figure 15 (A-weighted OASPL) shows that all of the noise components are underpredicted and that the broadband noise component is more important in this A-weighted metric. Similar to the level flight

case, the average noise metric level is lower than the OASPL level for this descent case. However, the rapid drop in A-weighted noise ahead of the rotor is not seen in the descent case. Effectively, the measured data shows that the OASPL and A-weighted metric time histories are simply offset by a constant in the vertical axis. This suggests that there is broadband content throughout the descent case, which is corroborated by the broadband content seen in the measured acoustic pressure time histories in Figure 12.

The predicted A-weighted OASPL trend is similar in shape to the measured A-weighted OASPL curve, with an offset in the vertical axis. This indicates that content in the frequencies emphasized by the A-weighting is underpredicted over the entire flyover.

6.4 PNLT and Time Integrated Metrics

Figure 16 shows the PNLT metric time history using data generated in the previous sections for the descent case. Again, predicted thickness noise dominates the PNLT on approach, loading noise is increasing as the vehicle approaches (and passes over) the microphone location; while, broadband noise is less important for this particular metric than are thickness or loading noise components.

Table 5 provides a summary of the measured and predicted integrated metrics. The column labeled "Pegg 91% Prediction" corresponds to the predicted column in Table 4 in that 91% of the Pegg broadband noise content in used. Later in this section, the effect of using a different scaling value for the Pegg model will be discussed.

Underprediction of the EPNL value shown in Table 5 is attributed to underpredicting the peak PNLT level just after the vehicle has passed the microphone. At t = 0 seconds, there is a large amount of broadband noise in the measured data (see the acoustic pressure time histories in Figure 12) that is not predicted, even with the Pegg broadband noise model included. The width of the integration window (10 dB below the peak on either side of the peak) is similar to the measured window.

The predicted unweighted SEL value is close to the measured value, though the peak noise (Lmax) is slightly lower than the measured value. Again, the integration window in determining SEL is similar to the measured window, but within the window OASPL is overpredicted and underpredicted resulting in a good predicted SEL value.

For the A-weighted quantities, there is significant underprediction of SEL and Lmax (Table 5) caused by underpredicting the noise components in the frequencies that are emphasized by the A-weighting. Based on Figure 15, underprediction of these A-weighted integrated metrics is expected. The main cause of underpredicting the A-weighted quantities is due to broadband noise underprediction.

Because of the underprediction of the A-weighted quantities and the recognition that some of this content is from broadband noise, Table 5

includes results from using a scaling factor of 1.0 for the Pegg broadband noise, rather than the 0.91 fraction that was derived from matching the A-weighted SEL in the level flight case. Using this larger scale factor improved the EPNL prediction with the error reduced by 50% compared to the results using a scale factor of 0.91. As expected, the unweighted values did not change much, as they are almost unaffected by the broadband content. The results in Table 5 suggest that for the descent case, the full Pegg model should be used.

Table 5. Summary of metrics for descent case.

		Pegg 91%		Pegg 100%	
	Measured	Predicted	% error	Predicted	% error
EPNL	93.67	92.41	-1.3	93.00	-0.7
unweighted					
SEL	99.93	99.71	$\approx 0.$	99.75	$\approx 0.$
Leq	90.15	90.20	$\approx 0.$	90.26	$\approx 0.$
Lmax	94.62	93.67	-1.0	93.67	-1.0
A-weighted					
SEL	92.10	86.47	-5.0	91.73	-0.4
Leq	82.07	78.54	-4.3	84.24	2.6
Lmax	85.47	81.95	-4.1	87.44	2.3

7 Conclusion

A noise prediction method consisting of a rotorcraft comprehensive analysis (CAMRAD II) that computes the vehicle trim state, blade motion, and blade loading was combined with a noise prediction code that utilizes ANOPP2 functionality to compute noise metrics. Various noise parameters and metrics were compared to measured data from a flight test.

The primary purpose of this effort was to examine the capability of the noise prediction method to reproduce features in the measured data, with the knowledge that the method could be incorporated into a rotor/rotorcraft design process. The design of a low-noise vehicle will probably examine representative noise metrics, such as EPNL and SEL, to trade against other vehicle attributes, such as speed and payload.

This work showed that measured data can be reasonably reproduced in terms of acoustic pressure time histories, 1/3-octave band sound pressure level spectra, PNLT time histories, and EPNL. For a level flight case, predictions of both unweighted and A-weighted metrics were representative of the measured values. For a descent case, predictions of the unweighted metrics were representative of the measured values; whereas, the predicted A-weighted metrics showed a 4 to 5% underprediction when the input parameters remained the same as those used for the level flight case. The measured descent case exhibited more broadband noise content for the entire flyover, and inclusion of more broadband noise in the prediction relative to the level flight case improved the comparison of integrated noise metrics. While the broadband noise model is a simple one based on scaling and empiricism, an improved broadband noise model could serve an important role in computing integrated metrics.

If only the noise from the main rotor is included, the integrated acoustic quantities for a main rotor / tail rotor vehicle will be significantly underpredicted. Inclusion of the tail rotor noise, though smaller than the main rotor noise in magnitude, is essential in the prediction method to compute many of the integrated noise metrics such as PNLT and EPNL due to the frequency content of the tail rotor. It was also shown that inclusion of a broadband noise model - even a simple empirical one - can modify, and even improve, the integrated metrics because broadband noise tends to dominate the time range of metric time history from which the integrated metrics (such as PNLT and EPNL) are computed.

The prediction method demonstrated that the comprehensive analysis for a given configuration can be "calibrated" once, then the "calibrated" model can be used for the remainder of reasonably similar cases. For this work, a level flight case served as the "calibration" case and the descent flight case was computed with the "calibrated" model. However, the level flight and descent cases had different levels of measured broadband noise. This difference was accounted for in the analysis by simply

scaling the results of an empirical broadband noise model. It is unclear whether this calibration method is valid for various flight conditions of the same vehicle or for vehicles of other size and weight classes.

As a next step in this research, vehicle variations will be examined using this same noise prediction method. For example, the above analysis could be repeated with various design changes, such as modification of the main rotor blade planform in such a way as to keep the vehicle in approximately the same trim state. This noise prediction method could also be inserted into a optimization framework such as OpenMDAO to minimize one of the acoustic quantities as an objective function.

8 Figures

8.1 Introduction

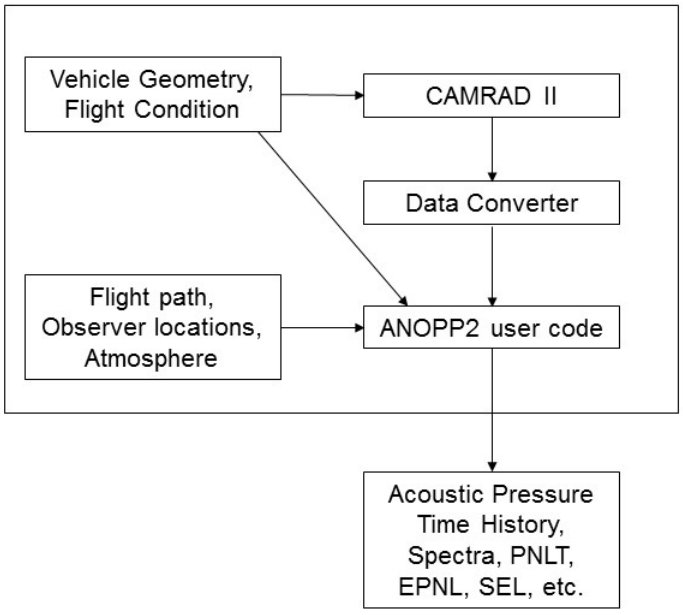

Figure 1. Outline of the current noise prediction method.

8.2 Level Flight

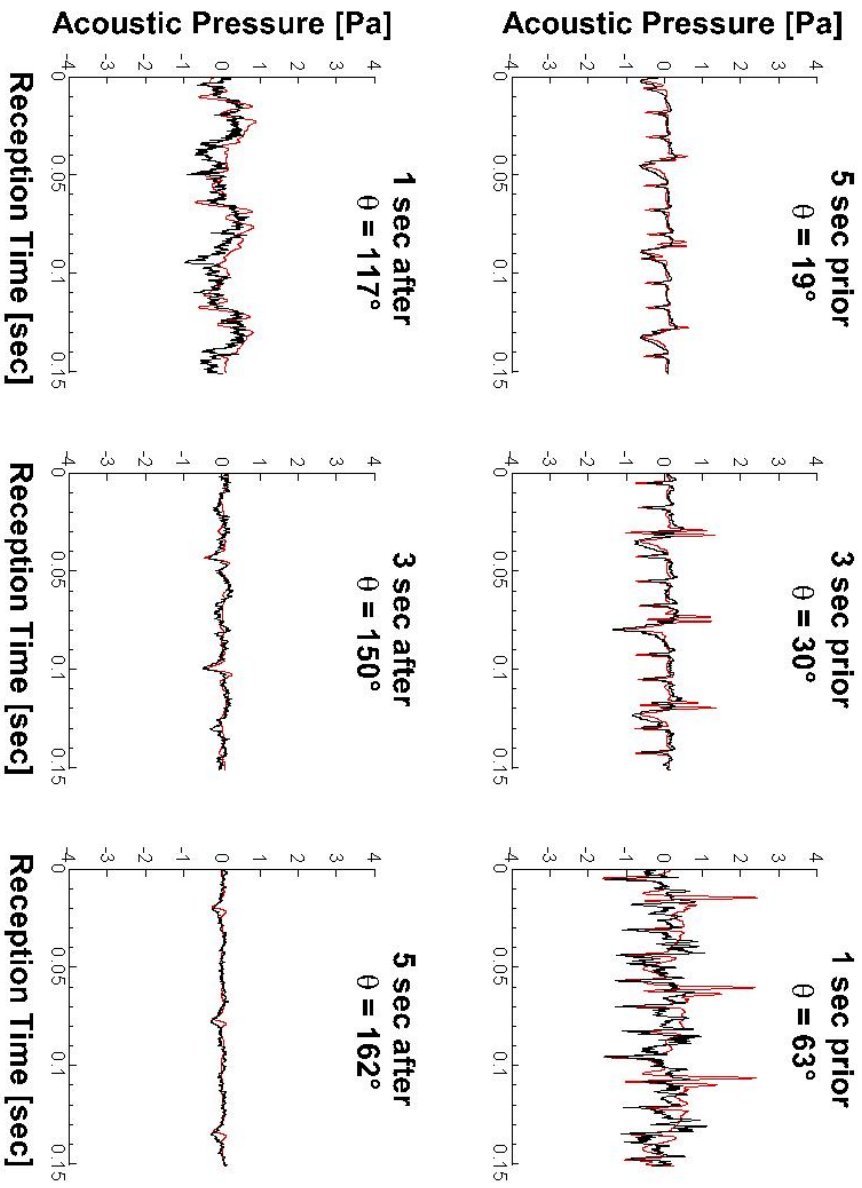

Figure 2. Level flight: Measured and predicted acoustic pressure from six points along the flight path. Red lines are predictions; black lines are measurements.

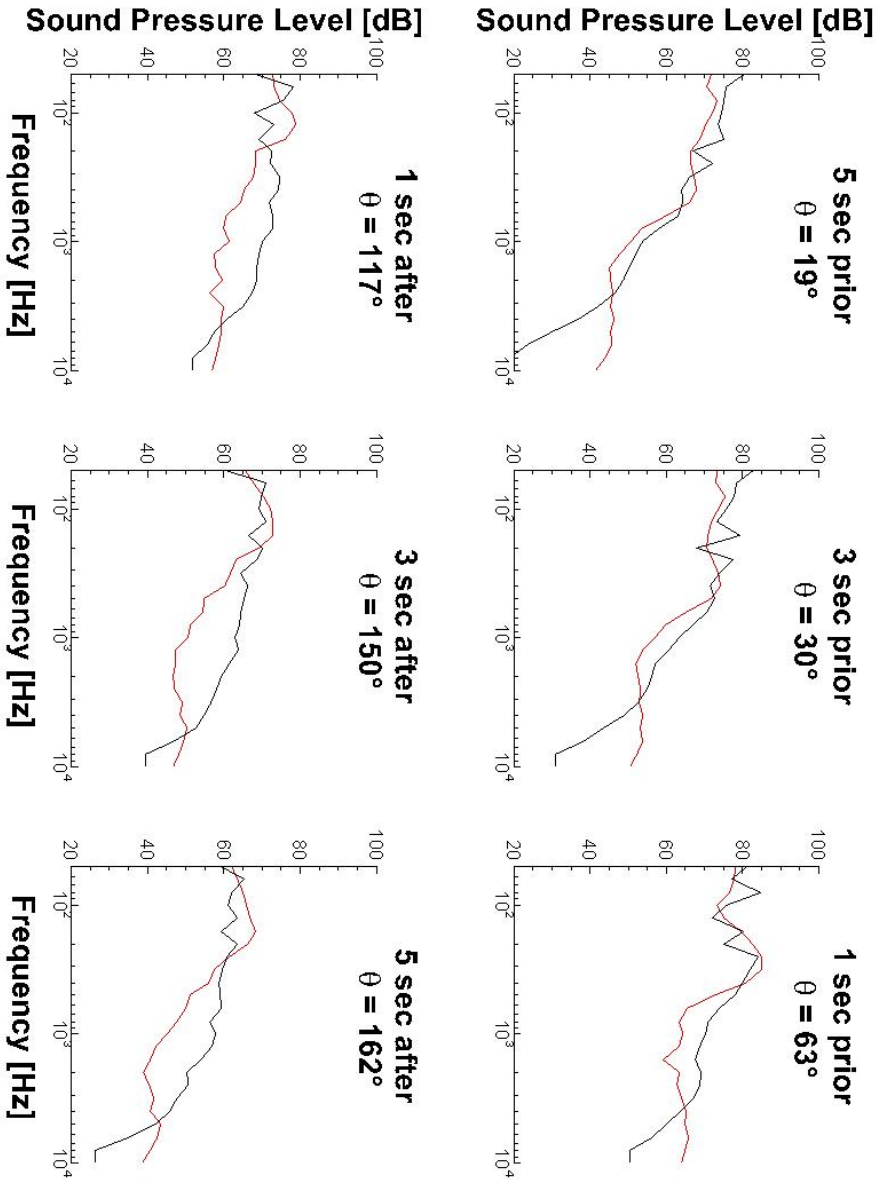

Figure 3. Level flight: Measured and predicted one-third octave band spectra at six points along the flight path. This prediction includes only the main rotor, but does not include broadband noise. Red lines are predictions; black lines are measurements.

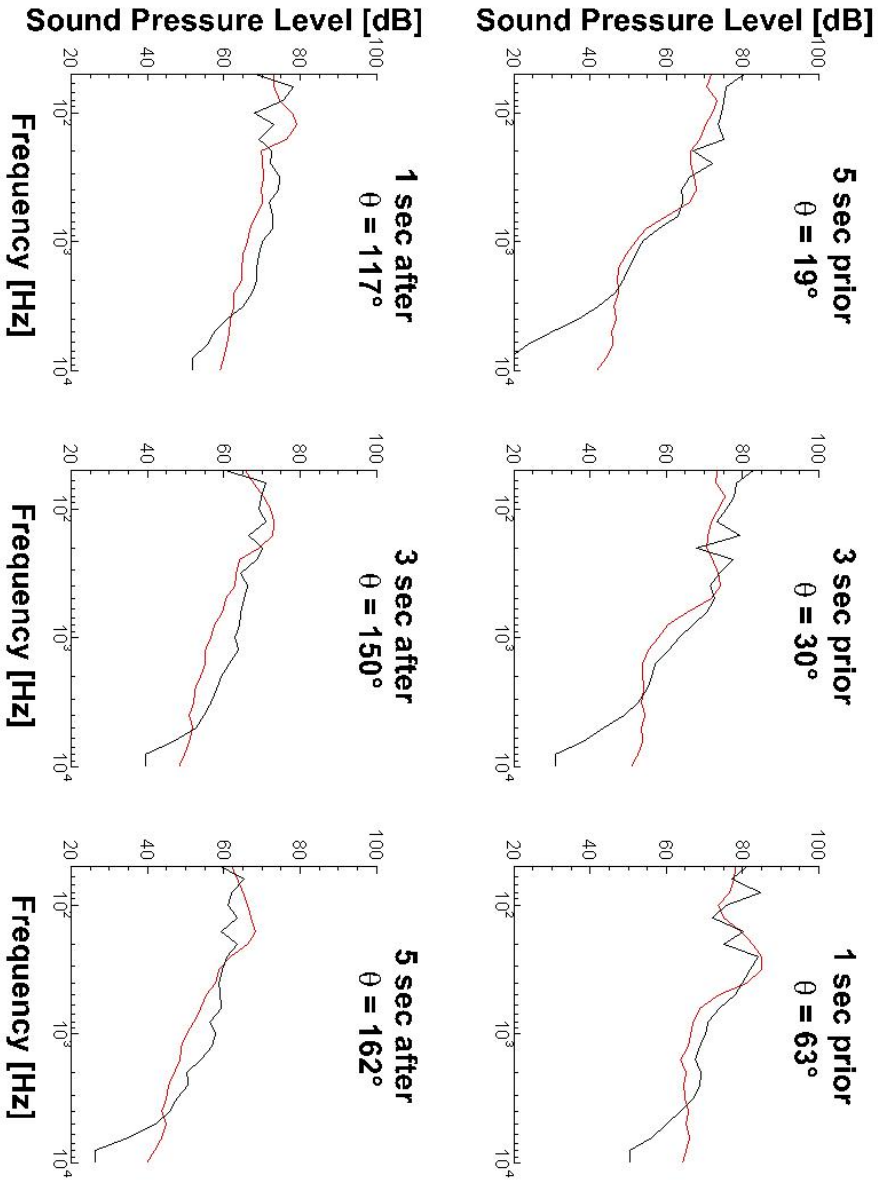

Figure 4. Level flight: Measured and predicted one-third octave band spectra at six points along the flight path. This prediction includes only the main rotor and includes broadband noise from the Pegg broadband noise model. Red lines are predictions; black lines are measurements.

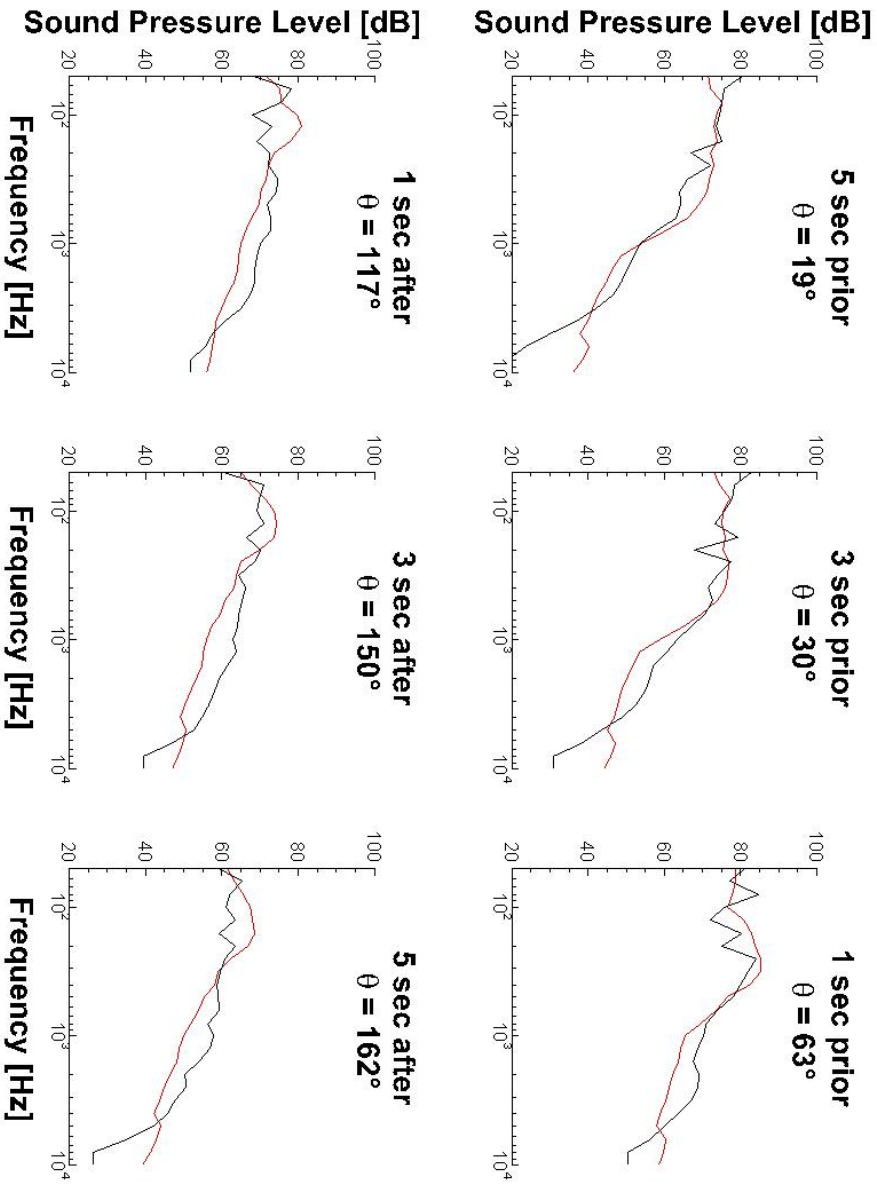

Figure 5. Level flight: Measured and predicted one-third octave band spectra at six points along the flight path. This prediction includes the main rotor (and its associated broadband noise from the Pegg broadband noise model) and tail rotor noise. Red lines are predictions; black lines are measurements.

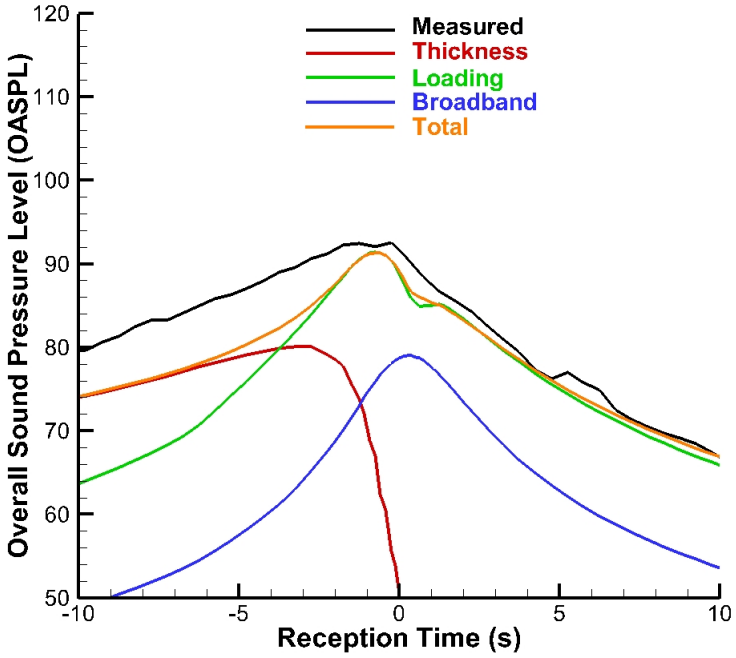

Figure 6. Level flight: Measured and predicted unweighted overall sound pressure level (OASPL) [dB]. This prediction includes the main rotor only.

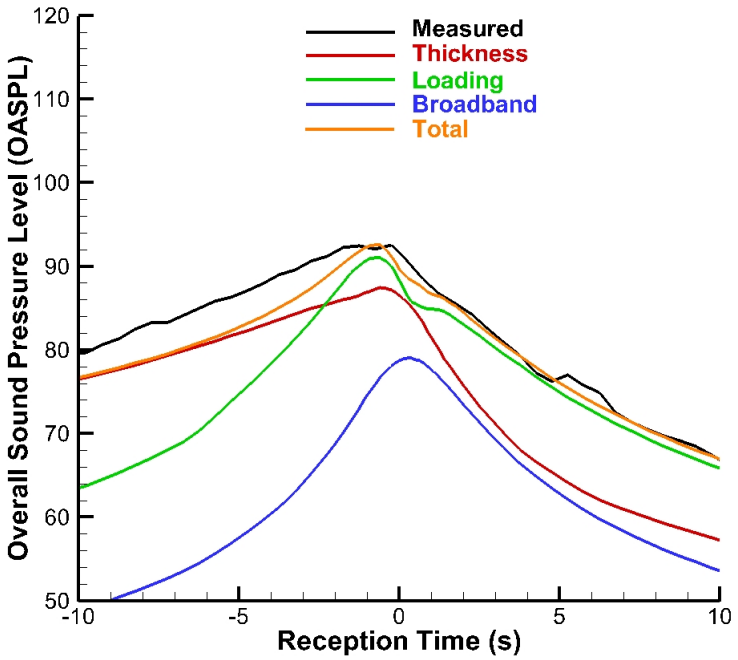

Figure 7. Level flight: Measured and predicted unweighted overall sound pressure level (OASPL) [dB]. This prediction includes both the main rotor and tail rotor.

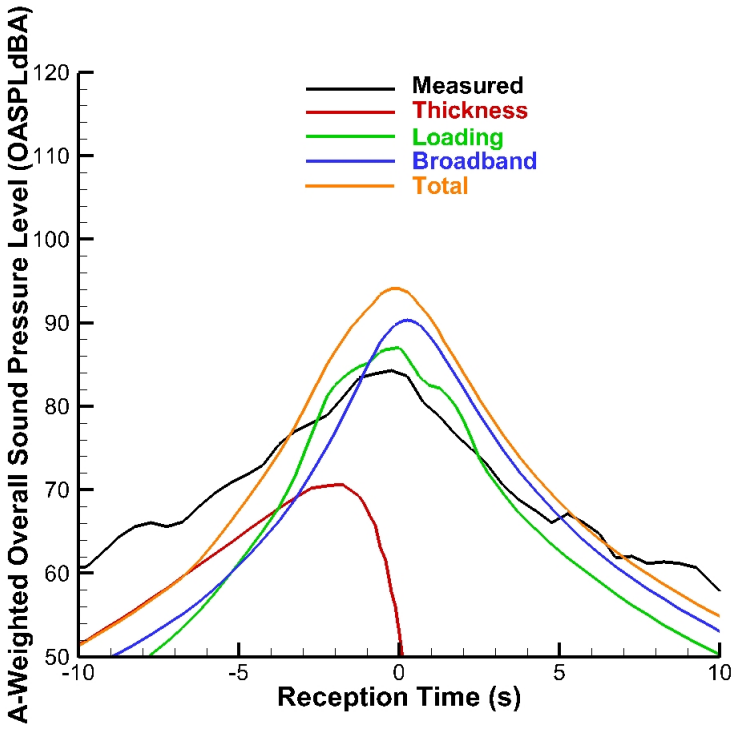

Figure 8. Level flight: Measured and predicted A-weighted overall sound pressure level (OASPL) [dBA]. This prediction includes the main rotor only.

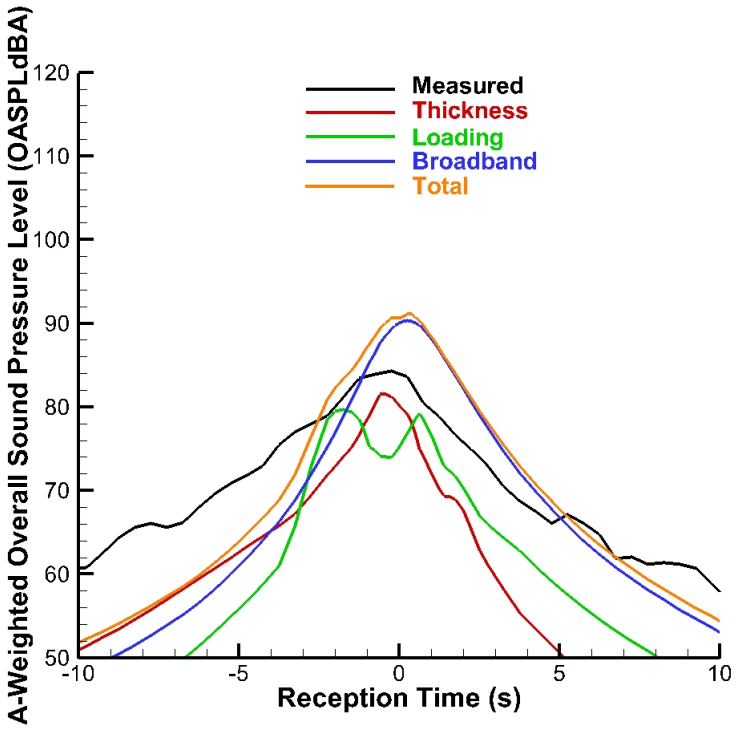

Figure 9. Level flight: Measured and predicted A-weighted overall sound pressure level (OASPL) [dBA]. This prediction includes both the main rotor and tail rotor.

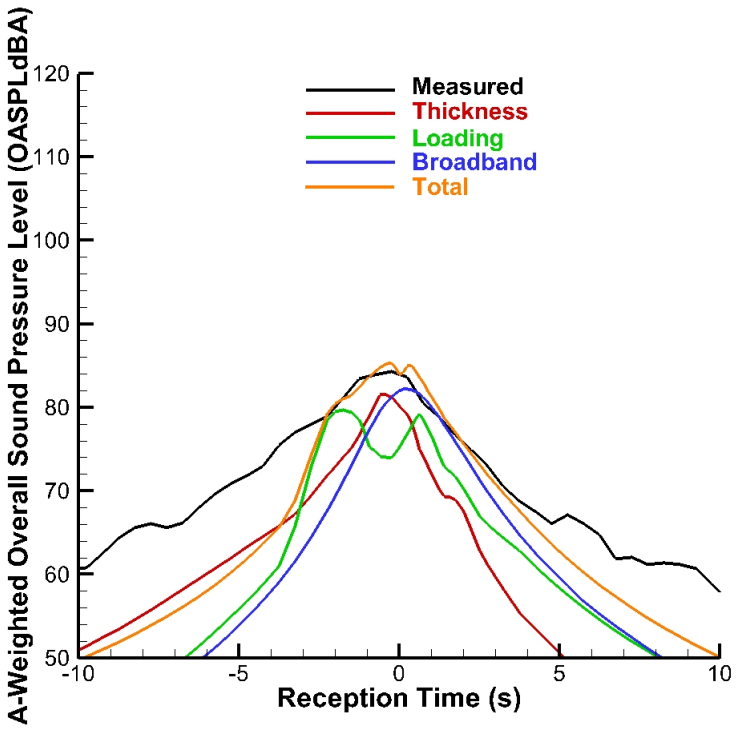

Figure 10. Level flight: Measured and predicted A-weighted overall sound pressure level (OASPL) [dBA]. This prediction includes both the main rotor and tail rotor. The broadband component has been reduced by 9%.

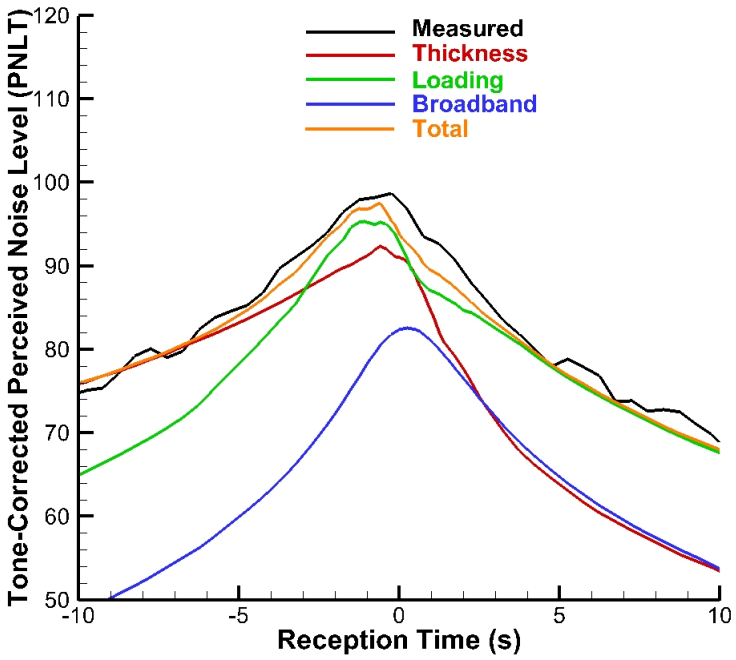

Figure 11. Level flight: Measured and predicted Tone Corrected Perceived Noise Level. This prediction includes the main rotor, main rotor broadband, and tail rotor noise.

8.3 Descent Flight

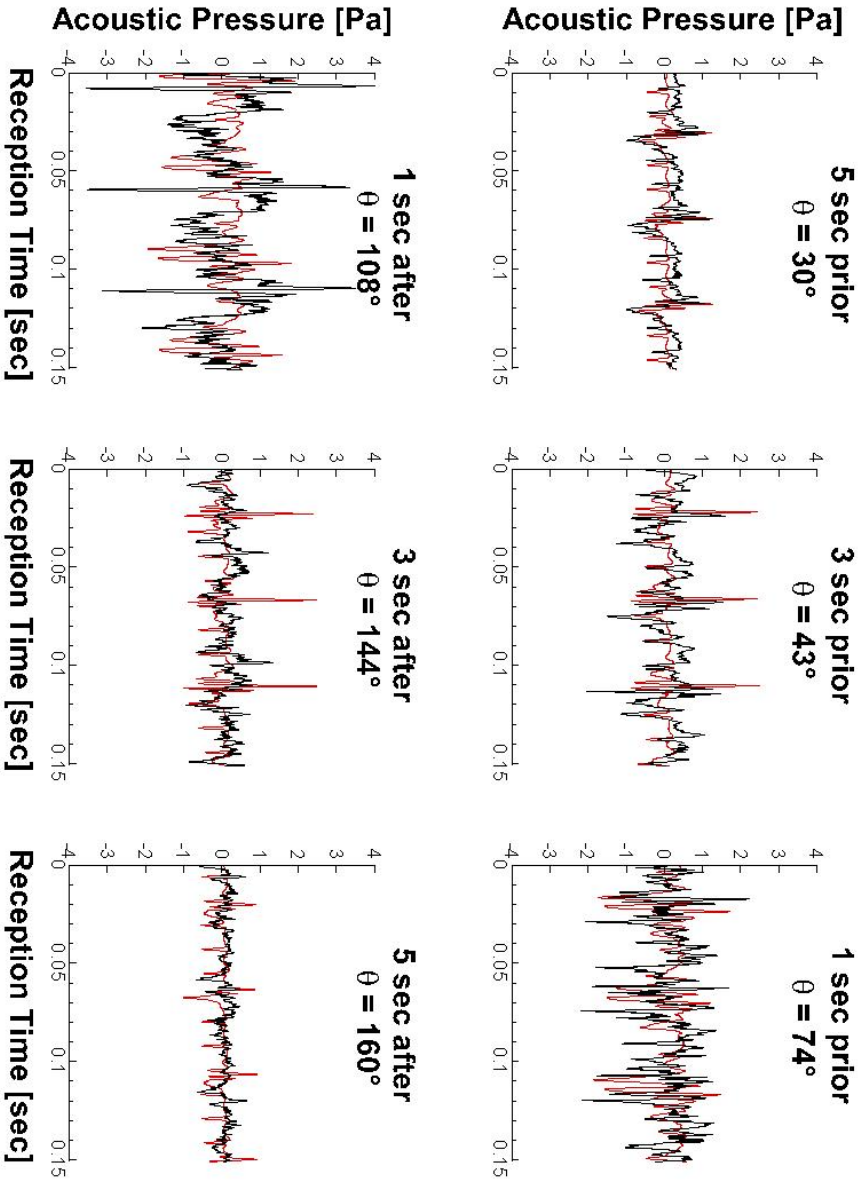

Figure 12. Descent flight: Measured and predicted acoustic pressure from six points along the flight path. Red lines are predictions; black lines are measurements.

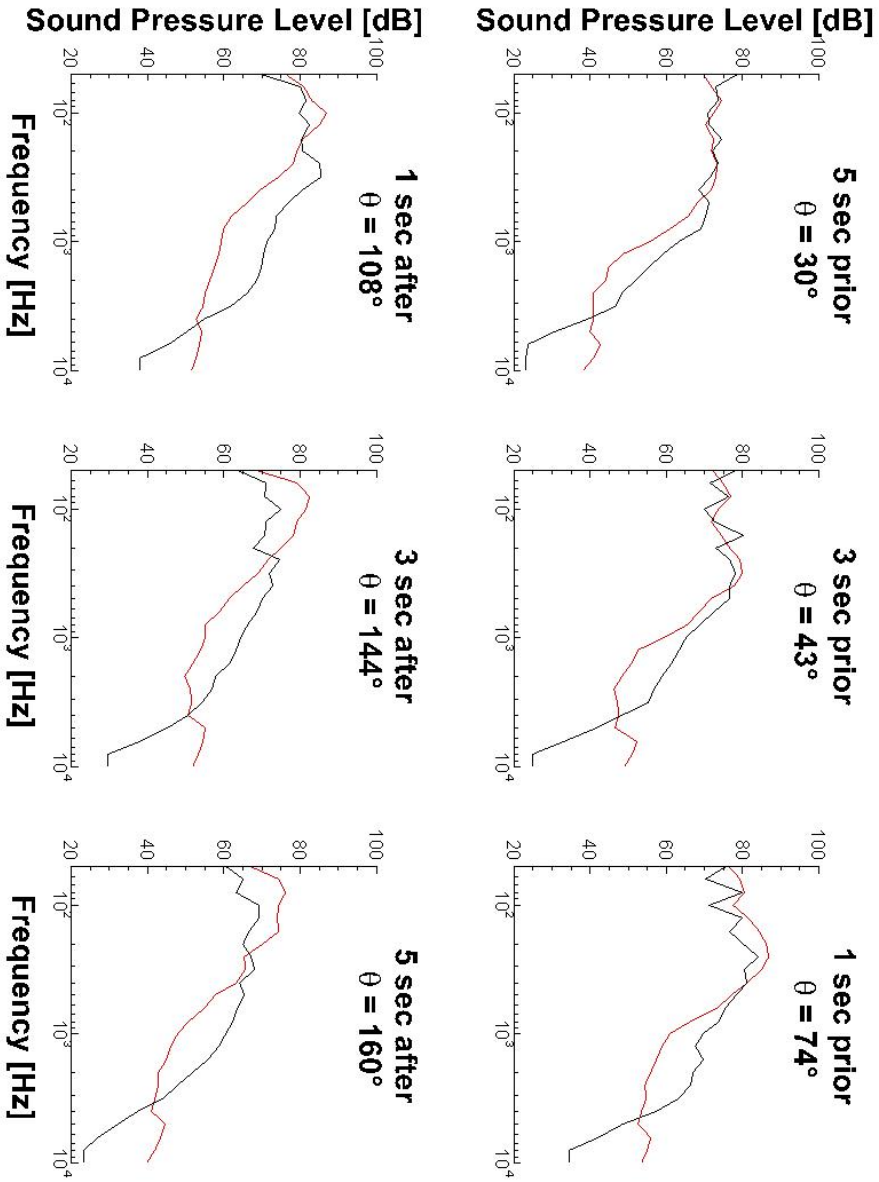

Figure 13. Descent flight: Measured and predicted one-third octave band spectra at six points along the flight path. This prediction includes the main rotor, main rotor broadband, and tail rotor noise. Red lines are predictions; black lines are measurements.

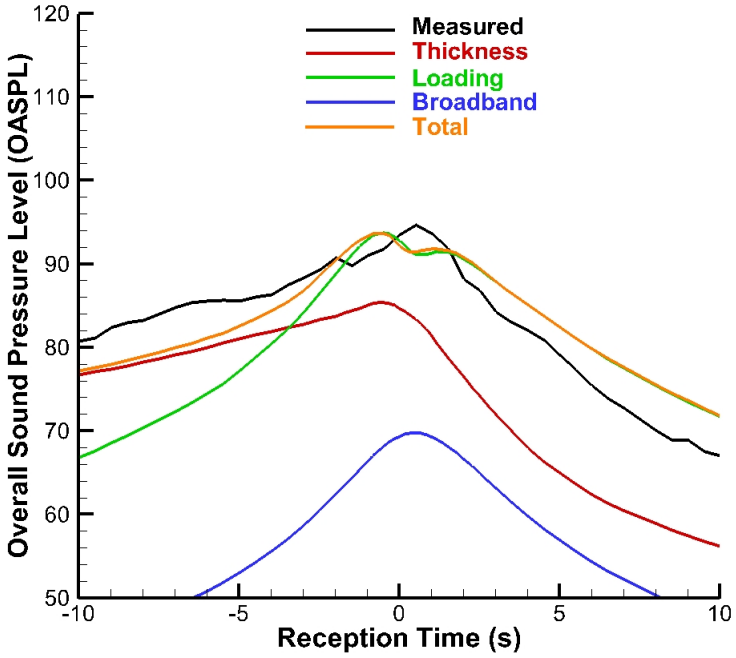

Figure 14. Descent flight: Measured and predicted unweighted overall sound pressure level (OASPL) [dB]. This prediction includes the main rotor, main rotor broadband, and tail rotor noise.

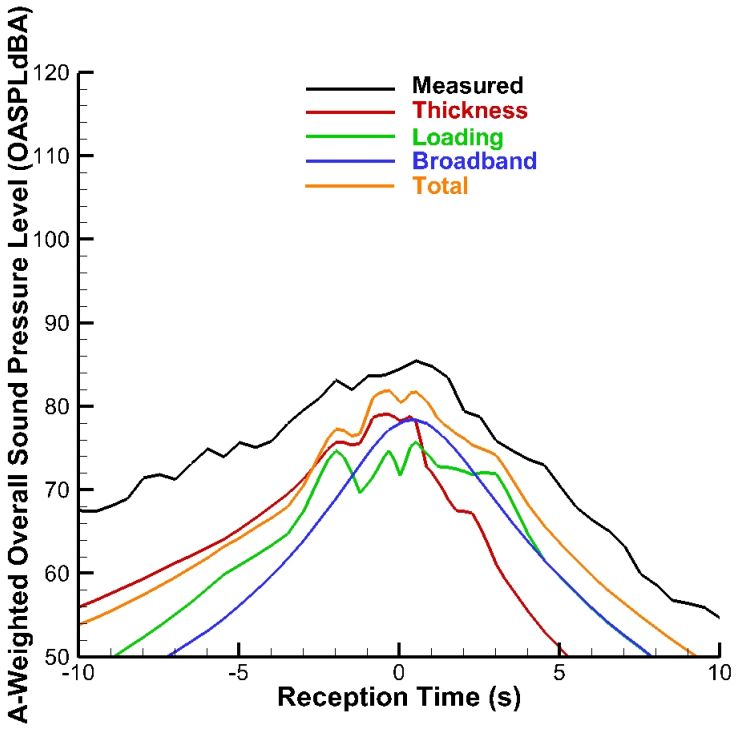

Figure 15. Descent flight: Measured and predicted A-weighted overall sound pressure level (OASPL) [dBA]. This prediction includes the main rotor, main rotor broadband, and tail rotor noise.

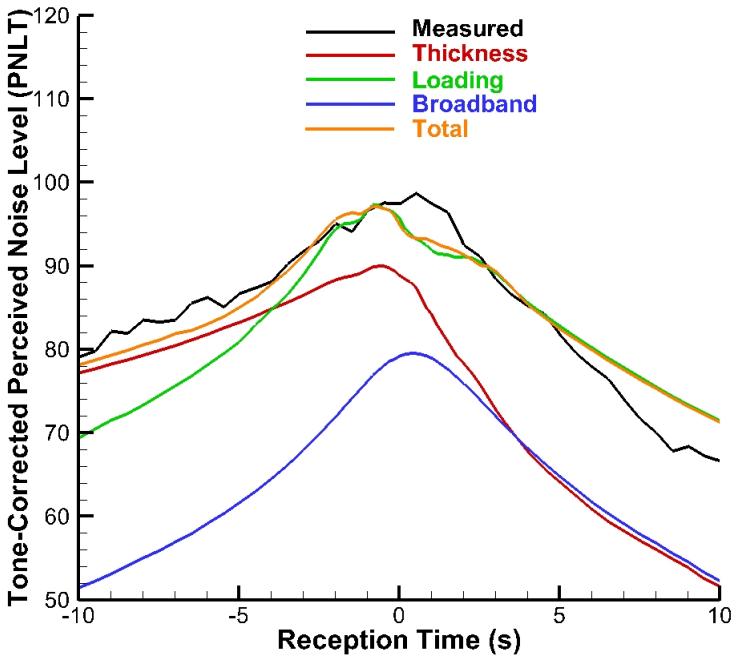

Figure 16. Descent flight: Measured and predicted Tone Corrected Perceived Noise Level. This prediction includes the main rotor, main rotor broadband, and tail rotor noise.

References

1. Johnson, W.R.: NDARC - NASA Design and Analysis of Rotorcraft - Theoretical Basis and Architecture. *American Helicopter Society Aeromechanics Specialists' Conference*, San Francisco, CA, January 20-22, 2010.

2. Heath, C.M., Gray, J.S.: OpenMDAO: Framework for Flexible Multidisciplinary Design, Analysis and Optimization Methods. *8th AIAA Multidisciplinary Design Optimization Specialist Conference (MDO)*, Honolulu, Hawaii, 2012, pp. 1–13.

3. Snider, R., Samuels, T., Goldman, B., Brentner, K.S.: Full-Scale Rotorcraft Broadband Noise Prediction and Its Relevance to Civil Noise Certification Criteria. *69th Annual American Helicopter Society International Forum*, Phoenix, AZ, May 21-23, 2013.

4. Johnson, W.R.: CAMRAD II: Comprehensive Analytical Model of Rotorcraft Aerodynamics and Dynamics (Version 4.9). *Johnson Aeronautics*, 2012.

5. Lopes, L.V., Burley, C.L.: ANOPP2 User's Manual. NASA/TM-2016-219342, October 2016.

6. Farassat, F.: Derivation of Formulations 1 and 1A of Farassat. NASA/TM-2007-21853, May 1, 2007.

7. Lopes, L.V.: Compact Assumption Applied to the Monopole Term of Farassat's Formulations. *21st AIAA/CEAS Aeroacoustics Conference*, Dallas, TX, June 22-26, 2015.

8. Pegg, R.J.: A Summary and Evaluation of Semi-Empirical Methods for the Prediction of Helicopter Rotor Noise. NASA TM 80200, May 1979.

9. Watts, M.E., Greenwood, E., Stephenson, J.H.: Measurement and Characterization of Helicopter Noise at Different Altitudes. *72nd American Helicopter Society International Forum*, West Palm Beach, FL, May 17-19, 2016.

10. Heffernan, R.M., Gaubert, M.: Structural and Aerodnamic Loads and Performance Measurements of an SA349/2 Helicopter with an Advanced Geometry Rotor. NASA TM 88370, November 1986.

11. Heffernan, R.M., Prescetti, D., Johnson, W.R.: Vibration Analysis of the SA349/2 Helicopter. NASA TM 102794, January 1991.

12. European Aviation Safety Agency: Operational Evaluation Board Final Report: Eurocopter Ecureuil / Single Engine Family (AS 350 B, D, B1, BA, BB, B3 and EC 130B4, T2), Revision 4. Köln, Germany, 2012.

REPORT DOCUMENTATION PAGE

Form Approved
OMB No. 0704–0188

1. REPORT DATE *(DD-MM-YYYY)*	2. REPORT TYPE	3. DATES COVERED *(From - To)*
01-01-2017	Technical Memorandum	

4. TITLE AND SUBTITLE
Examination of a Rotorcraft Noise Prediction Method and Comparison to Flight Test Data

5a. CONTRACT NUMBER

5b. GRANT NUMBER

5c. PROGRAM ELEMENT NUMBER

6. AUTHOR(S)
Boyd, Jr., D. Douglas, Greenwood, Eric, Watts, Michael E., Lopes, Leonard V.

5d. PROJECT NUMBER

5e. TASK NUMBER

5f. WORK UNIT NUMBER
664817.02.07.03.02.01

7. PERFORMING ORGANIZATION NAME(S) AND ADDRESS(ES)
NASA Langley Research Center
Hampton, Virginia 23681-2199

8. PERFORMING ORGANIZATION REPORT NUMBER
L–20781

9. SPONSORING/MONITORING AGENCY NAME(S) AND ADDRESS(ES)
National Aeronautics and Space Administration
Washington, DC 20546-0001

10. SPONSOR/MONITOR'S ACRONYM(S)
NASA

11. SPONSOR/MONITOR'S REPORT NUMBER(S)
NASA-TM–2017–219370

12. DISTRIBUTION/AVAILABILITY STATEMENT
Unclassified-Unlimited
Subject Category 64
Availability: NASA STI Information Desk at 757-864-9658

13. SUPPLEMENTARY NOTES
An electronic version can be found at http://ntrs.nasa.gov.

14. ABSTRACT
With a view that rotorcraft noise should be included in the preliminary design process, a relatively fast noise prediction method is examined in this paper. A comprehensive rotorcraft analysis is combined with a noise prediction method to compute several noise metrics of interest. These predictions are compared to flight test data. Results show that inclusion of only the main rotor noise will produce results that severely underpredict integrated metrics of interest. Inclusion of the tail rotor frequency content is essential for accurately predicting these integrated noise metrics.

15. SUBJECT TERMS
Acoustics, Noise, Rotorcraft, Helicopter

16. SECURITY CLASSIFICATION OF:			17. LIMITATION OF ABSTRACT	18. NUMBER OF PAGES	19a. NAME OF RESPONSIBLE PERSON
a. REPORT	b. ABSTRACT	c. THIS PAGE			STI Information Desk (email: help@sti.nasa.gov)
U	U	U	UU	48	19b. TELEPHONE NUMBER *(Include area code)* 757-864-9658